



DEPARTMENT OF INFORMATICS

TECHNISCHE UNIVERSITÄT MÜNCHEN

Master's Thesis in Robotics, Cognition, Intelligence

Comparison of Controllers for Trunk Stabilization in a Bipedal Robot

Felix Schausberger





DEPARTMENT OF INFORMATICS

TECHNISCHE UNIVERSITÄT MÜNCHEN

Master's Thesis in Robotics, Cognition, Intelligence

Comparison of Controllers for Trunk Stabilization in a Bipedal Robot

Vergleich von Reglern für die Rumpfstabilisierung in einem zweibeinigen Roboter

Author:	Felix Schausberger
Supervisor:	Prof. dr. ir. Daniel J. Rixen
Advisor:	Dr.-Ing. Daniel Renjewski
Submission Date:	15.03.2023



I confirm that this master's thesis in robotics, cognition, intelligence is my own work and I have documented all sources and material used.

Munich, 15.03.2023

Felix Schausberger

Acknowledgments

Firstly I would like to thank my advisor Dr. Ing. Daniel Renjewski for his dedicated involvement and support through the past few months. He made this thesis possible in the first place. Furthermore, I want to thank Julian Schausberger as the second reader of this thesis for his open ears and insightful comments. I would also like to offer my gratitude to my friend, Lilla Nagy, who I collaborated with through the years while at Technical University of Munich (TUM). Thank you for always being dependable and I wish you all the best in your academic pursuits. A big thank you to Melina Neuß for always being available to supply me with the parts and the laughs needed to get through this project. Lastly but most importantly, I am eternally grateful to my parents, Klaus and Brigitta Schausberger, who have always given me a free hand in my career decisions and supported me in everything I have done. Thank you.

Abstract

Balancing the trunk on long legs is a major challenge in bipedal walking. To avoid conflicting control objectives, all aspects of gait control must be tightly integrated. The goal of this thesis is to quantify and analyze the similarities and differences between different control strategies and test them on a robotic testbed. In the course of this work, a review of approaches to torso stabilization in bipedal robots will be given first. A corresponding controller will then be implemented and simulated in a computer model. Finally, quantitative parameters are determined to evaluate the controller.

Zusammenfassung

Das Ausbalancieren des Rumpfes auf langen Beinen stellt eine große Herausforderung beim zweibeinigen Gehen dar. Um Zielkonflikte bei der Steuerung zu vermeiden, müssen diese mit allen anderen Aspekten der Steuerung des Gehens eng verzahnt werden. Ziel dieser Arbeit ist es, die Gemeinsamkeiten und Unterschiede zwischen verschiedenen Kontrollstrategien zu quantifizieren, zu analysieren und auf einem Roboterprüfstand zu testen. Im Zuge dieser Arbeit wird zuerst eine Übersicht über Ansätze zur Rumpfstabilisierung bei zweibeinigen Robotern geben. Ein entsprechender Regler wird anschließend in einem ComputermodeLL implementiert und simuliert. Abschließend werden quantitativen Parameter ermittelt, um den Regler zu bewerten.

Contents

Glossary	xii
Acronyms	xiv
1 Introduction	1
2 Fundamentals	2
2.1 Gaits	2
2.1.1 Symmetrical vs. Asymmetrical Gaits	2
2.1.2 Bipedal Gaits	4
2.2 Gait Analysis	4
2.2.1 Spring-Loaded Inverted Pendulum	4
2.2.2 Rigid Inverted Pendulum	5
2.2.3 Bipedal Spring-Loaded Inverted Pendulum	6
2.2.4 Mechanical Cost Analysis	6
2.3 Summary	9
3 Solution approach	10
3.1 The JenaFox Bipedal Walking Robot	10
3.2 Neural Network Controller	11
3.3 Vertical Leg Orientation	15
3.4 Trajectory Optimization	15
3.5 Summary	19
4 Evaluation	20
5 Future work	22
6 Conclusion	23
A Appendix 1	24
Bibliography	25

List of Figures

2.1	Common gaits of bipeds (a, c) and quadrupeds (b, d). Stereotypical foot contact phases are represented as a fraction of stride period on polar plots. The outer ring represents the rear limb contacts (blue) and the inner ring represents the front limb contacts (green). Half a cycle out of phase of fore and hind legs indicates symmetrical gait (a, b), substantial deviations of this in either pair indicates asymmetrical gait (c, d). (Adapted from [24], p. 3)	3
2.2	Schematic representation of the stance-phase pattern with its characteristic m-shape of the vertical GRF of a bipedal spring-mass model. The steady-state solution starts at heel strike, has a local minimum at mid-stance and ends at toe-off.	5
2.3	Schematic representation of the mechanical cost analysis (MCA) for a compliant SLIP (a) as well as the idealized zero-collision case (b). Shown are the force vector F and velocity vector V with their corresponding angles, θ and λ of two isolated, hypothetical strides. The collision angle ϕ is the deviation of the orthogonal relation between F and V . The collision reduction is quantified by the collision fraction κ . (Adapted from [22], p. 4)	7
3.1	Schematic representation of the JenaFox bipedal walking robot (a) with associated planes of motion (b). The bipedal robot consists of a torso connected to two segmented legs, each of which has an upper and a lower link. The X-axis (orange) points in the direction of motion, the Y-axis (green) points upward. The trunk of the robot is attached to a boom via a freely rotating joint which constrains the motion of the robot on a sphere. The planar motion is thus restricted to the sagittal plane (orange).	11
3.2	The control parameters for the hip (a) extensor $\theta_{ES,h}$ (orange) and flexor $\theta_{FS,h}$ (blue) as well as the knee (b) extensor $\theta_{ES,k}$ (orange) and flexor $\theta_{FS,k}$ (blue) joint angles according to the International Society of Biomechanics (ISB) convention. (Adapted from [31])	13
3.3	Graphical representation of equation 3.1. The sigmoid function maps the projected velocity vector λ_{proj} to obtain the anterior extreme angle (AEA).	13
3.4	Graphical representation of equation 3.1. The sigmoid function maps the projected velocity vector λ_{proj} to obtain the anterior extreme angle (AEA).	14
3.5	The bipedal spring mass model for walking. The simulation starts at the moment of vertical leg orientation (VLO) during single support phase (VLO ₀) and ends after one step is completed at VLO of the opposite leg (VLO ₁). (Adapted from [33], p. 1)	15

3.6	Degrees of freedom of the basic mechanical setup. The trunk (mass m_b) has three degrees of freedom (q_1, q_2, q_3), hip and knee of the right leg connect the thigh (m_t) to the body and shank (m_s) to the thigh respectively by one degree of freedom each (q_4, q_5), the same counts for the left side (q_6, q_7). (Adapted from [29], p.37)	17
4.1	The velocity vectors at touchdown. At the beginning of the velocity vectors the leg position is schematically shown, where the hip, knee and ankle joints are drawn as circles. From this it can be seen that the robot performs the touchdown with a fully extended knee. The colors refer to the different motor gains, with red representing the lowest with a GM_h of 1, and purple the highest with a GM_h of 1.8.	21
4.2	The velocity vectors at VLO. At the beginning of the velocity vectors the leg position is schematically shown, where the hip, knee and ankle joints are drawn as circles. A single step is completed when the swing leg attains ground contact and the CoM is orthogonally above the second foot point ($x = x_{FP_2}$). The colors refer to the different motor gains, with red representing the lowest with a GM_h of 1, and purple the highest with a GM_h of 1.8.	21

List of Tables

3.1	Solver settings for the JenaFox robot MATLAB Simulink simulation.	11
3.2	Overview of the control scheme used for the JenaFox robot. Touchdown and reaching the anterior extreme angle (AEA) of either hip angle triggers the corresponding action. When the target is reached the power of the moving motors is switched off. In the images, the events are shown as dark stick figures and the corresponding actions as light stick figures. (Adapted from [29], p.36)	12
3.3	Overview of the used control parameters for the sensory neurons, i.e. the joint angles of the hip extensor $\theta_{ES, h}$ and flexor $\theta_{FS, h}$ as well as the knee extensor $\theta_{ES, k}$ and flexor $\theta_{FS, k}$	14
3.4	Overview of the used control parameters for the motor neurons. τ is a time constant associated with the passive properties of the cell membrane, M_{AMP} represents the magnitude of the servo amplifier. GM_h and GM_k depict the gain of the hip and knee motor, respectively.	14
3.5	Initial condition used in the multi-body simulation consisting of the hip and knee angles of the swing leg, $\phi_{IC, hr}$ and $\phi_{IC, kr}$, the angle of the torso $\phi_{IC, torso}$ as well as their corresponding velocities $\dot{\phi}_{IC, hr}$, $\dot{\phi}_{IC, kr}$ and $\dot{\phi}_{IC, torso}$	18
3.6	Identified failure modes of the system which may occur. A total of 6 failure modes were identified, the CoM or one of the knees falling below a threshold in height, the robot starting to walk backwards as well as reaching a time or distance limit. If any of these cases occur, the simulation is aborted and the cost is penalized with a penalty function.	19

Glossary

F Vector of the ground reaction force, i.e. the external force acting on the limb (N). ix, xii, 7, 8, 9

Fr Froude number. 8

GM Motor gain. x, xi, 14, 20, 21

M_{AMP} Magnitude of the servo amplifier. xi, 14

P_{mech} Power of the limb acting on the center of mass of the body, i.e. the external mechanical power (J). 7, 8

V Velocity vector of the center of mass ($\frac{m}{s}$). ix, xii, 7, 8, 9

W_{mech} External mechanical work (W). 8

Λ Average angle associated with V ($^{\circ}$). xii, 9

Φ Average collision angle ($^{\circ}$). xii, 8, 9

Θ Average angle associated with F ($^{\circ}$). xii, 9

α_{TD} Angle of attack ($^{\circ}$). 13, 20

$\dot{\phi}_{IC}$ Initial condition of \dot{q} used in the multi-body simulation. xi, 18

κ Collision fraction, calculated as the quotient of Φ and the sum of Λ and Θ . ix, 7, 9

λ Instantaneous angle of V relative to horizontal ($^{\circ}$). ix, 7, 9, 13, 14, 20

ϕ Instantaneous angle of deviation of perpendicularity of force and velocity vectors (collision angle) ($^{\circ}$). ix, 7, 8, 9

ϕ_{IC} Initial condition of q used in the multi-body simulation. xi, 18

τ Time constant associated with the passive properties of the cell membrane (s). xi, 14

θ Instantaneous angle of F relative to vertical ($^{\circ}$). ix, 7, 9

θ_{ES} Control parameter of the extensor for the neural controller ($^{\circ}$). ix, xi, 13, 14

θ_{FS} Control parameter of the flexor for the neural controller ($^{\circ}$). ix, xi, 13, 14

d Offset, i.e. the intersection of the line with the y-axis. 13, 20

g Acceleration due to gravity ($\frac{m}{s^2}$). 8

h Height of the center of mass. 8

- k Constant of proportionality, which relates two variables in a direct variation. 13
- m Mass of the body (kg). 8
- n Number of sampled points in a stride period. 8
- q Cumulative vector containing the DoF of the system. x, xii, 17, 18

Acronyms

AEA Anterior Extreme Angle ix, xi, 12, 13, 14, 20

BSLIP Bipedal Spring-Loaded Inverted Pendulum 5, 6

CoM Center of Mass x, xi, xii, 2, 4, 5, 7, 8, 9, 13, 14, 15, 18, 19, 20, 21

CoT Cost of Transport 18

CoT_{mech} Mechanical Cost of Transport 6, 8

DoF Degrees of Freedom xiii, 17

GRF Ground Reaction Force ix, ~~xii~~, 4, 5, 6, 7

ISB International Society of Biomechanics ix, 12, 13

MCA Mechanical Cost Analysis ix, 6, 7, 9

NLP Nonlinear Program 16

PEA Posterior Extreme Angle 12

RIP Rigid Inverted Pendulum 4, 5, 6, 9

SLIP Spring-Loaded Inverted Pendulum ix, 2, 4, 5, 6, 7, 9

TUM Technical University of Munich iii

VLO Vertical Leg Orientation ix, x, 10, 15, 16, 17, 18, 19, 20, 21

Chapter 1

Introduction

Robotics aims to build artificial cognitive systems that can act on their own to achieve some predefined goal. However, in order to be able to respond to and interact with one's environment, the necessity of grasping basic mechanisms of our world evolves. To master this, agents¹ are required to perceive their environment, anticipate the need to act, learn from experience, and adapt to changing circumstances. Robots must navigate an increasingly complex, uncertain, unstructured and human-shaped environment. This can only be achieved by exhibiting some degree of cognition. [36] Hereby, nature provides a remedy. The course of millions of years of evolution created an almost inexhaustible arsenal of potential solutions and highly optimized system processes, which frequently inspire engineers. [34] Studies of mechatronic systems inspired by biology can be categorized in respects of locomotion and mechanisms, actuation, sensing, and control [35]. Especially nature's ways of mastering locomotion provide a myriad of inspirations as nature has evolved various biological forms and functions to maneuver energy efficiently, agilely and safely through even the most hazardous environments. Locomotion is equally fundamental to all living things for foraging, catching prey, evading predators, protecting territory, finding mates, and migrating. For mankind in particular, it has played a central role in hunting, agriculture, transportation, sports, and warfare. [24] As with any structurally or functionally occurring feature in nature, it is important to analyze locomotion through the lens of organic evolution, as it emerged through the process of natural selection rather than the straightforward process of engineering. Subsequently, two types of terrestrial locomotion established in nature: walking upright on at least two legs like humans and most mammals do, which facilitates fast locomotion; and crawling low over the ground like reptiles, which usually tends to greater stability especially on rough terrain. [35] Hereby, energy comes at a premium not only for living creatures but also for robots, which need to carry sufficient energy in their batteries. Although the energy of a robot is consumed at many levels, from the control systems to the actuators, Lee and Harris [24] assume that the mechanical cost of transport is an integral energy cost for any legged system. Measuring this consumption allows the most direct comparison between the gaits of legged creatures and robots. Although legged robots have equaled or even surpassed the total cost of transport of legged creatures, this is usually only achieved by choosing extremely slow speeds or by using regenerative mechanisms. [24]

¹Respectively any artificial entity displaying some degree of cognition [36].

Chapter 2

Fundamentals

The analysis of terrestrial locomotion in the last half century has focused mainly on strategies for mechanical energy recovery during walking and running [22]. As early as the mid-1960s, Hildebrand [14] and others used cine films to distinguish gaits of terrestrial animals by such means as the duty cycle or limb contact phases. About a decade later, Cavagna, Heglund, and Taylor [5] revolutionized the understanding of animal locomotion by defining center of mass (CoM) mechanics using a point mass model and force plate measurements of the whole animal. Their comparison of walking and running reduced gait complexity by proposing that separate and mutually exclusive mechanisms act to exchange energy during the gait phase, such as anti-phase to in-phase kinetics and potential energy fluctuations. The publication induced today's widely accepted paradigm of conceptualizing walking as a rigid inverted pendulum and running as a compliant spring-loaded inverted pendulum (SLIP). [23] While walking, the mechanical energy of the CoM remains nearly constant as kinetic and potential energies interchange ~~oscillatory~~, causing the CoM to ascend over the support limb in mid-stance and fall forward into the next step. During running, however, this exchange is not possible because the CoM attains its lowest point in mid-stance, where the kinetic energy is also low. For this reason, ~~running gaits assume the use of a spring-mass mechanism~~ in which the interaction between the CoM and the ground allow for the storage and return of elastic strain energy in rather compliant legs. [22]

2.1 Gaits

Over millions of years of evolution, living creatures have developed various modes of locomotion, so-called gaits, which can be distinguished by their movement, i.e. their temporal footfall patterns. For terrestrial animals, the footfall sequence represents the primary identifying feature of their gait, quantified by the phase relationship of the individual legs and expressed as a fraction or percentage of the time of foot contact to the stride¹ period. For example, in bipedal walking, one foot lands at the beginning of the stride (i.e. at 0%) and the second foot lands at mid-stride (i.e. at 50%), representing one entire step. [24]

2.1.1 Symmetrical vs. Asymmetrical Gaits

Legged gaits can be classified as symmetrical and asymmetrical, according to the phase relationship of the left-right pairs of legs, regardless of the number of pairs. If the left and

¹A stride consists of two consecutive steps.

right leg of a pair is one-half stride cycle apart out of phase, the gait is defined as symmetrical - if not, the gait is defined as asymmetrical. Examples of a symmetrical gait include the bipedal walking of humans, the quadrupedal trotting of dogs, the pacing of camels, and the six-legged trotting of cockroaches, where all left-right pairs of front, middle, and hind legs are one-half stride cycle out of phase with one another. The number of legs limits the number of leg sequencing options, such that bipedal striding gaits are restricted to symmetric (walking and running, see fig. 2.1a) and asymmetric gaits (hopping and skipping, see fig. 2.1c). Quadrupeds use five symmetrical gaits (lateral and provisional diagonal sequence walking, trotting (see fig. 2.1b), pacing and ambling) and six asymmetrical gaits (lope, transverse and rotary gallops, half-bound (see fig. 2.1d), bound, and pronk). [24] However, note that these are broad definitions and that phase separations between foot contacts show substantial variation within gaits, as can be seen in Hildebrand's [14], [15] plots for the gaits of horses and dogs. In summary, the difference between symmetrical and asymmetrical gaits lies in the coordination of the legs, with symmetrical gaits involving both legs on the same side moving together and asymmetrical gaits involving diagonal pairs of legs moving together.

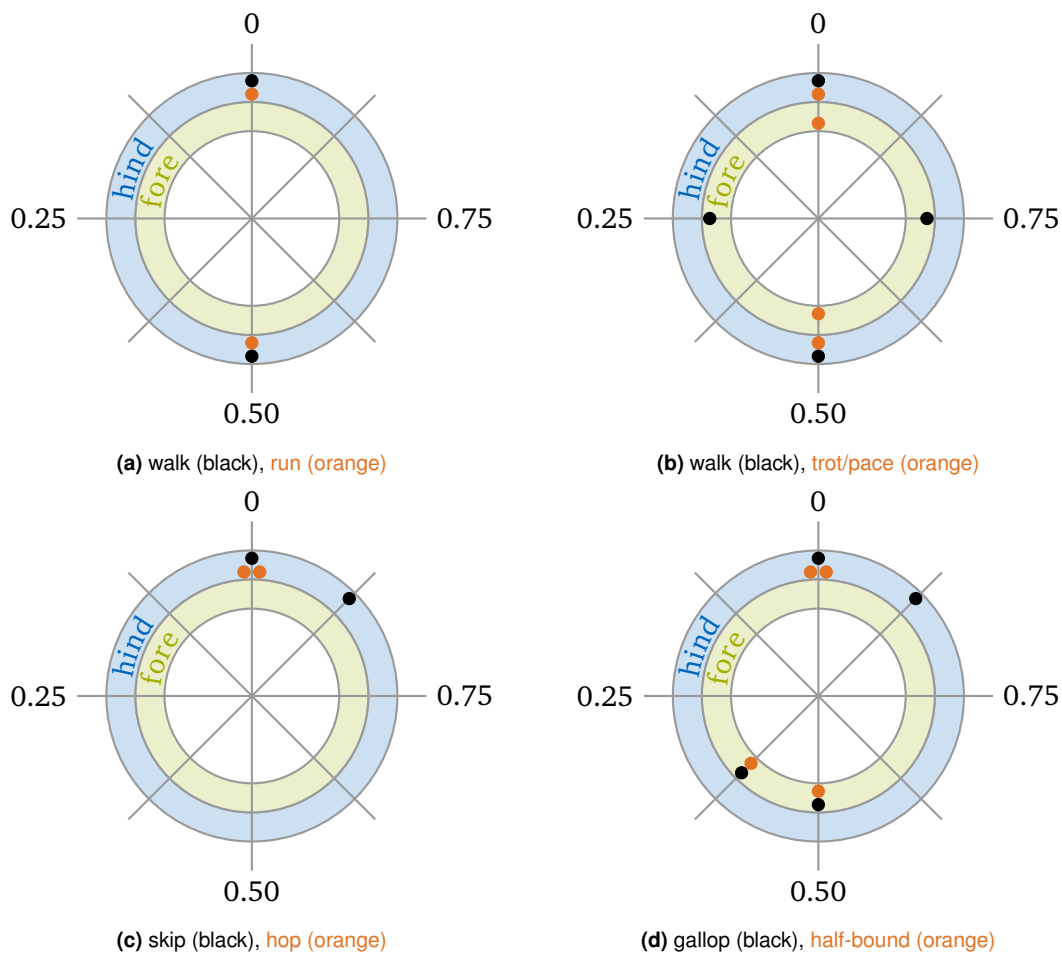


Figure 2.1: Common gaits of bipeds (a, c) and quadrupeds (b, d). Stereotypical foot contact phases are represented as a fraction of stride period on polar plots. The outer ring represents the rear limb contacts (blue) and the inner ring represents the front limb contacts (green). Half a cycle out of phase of fore and hind legs indicates symmetrical gait (a, b), substantial deviations of this in either pair indicates asymmetrical gait (c, d). (Adapted from [24], p. 3)

2.1.2 Bipedal Gaits

Bipedal striding gaits, including that of ~~our own genus~~, are symmetrical by definition 2.1a. Biomechanically, bipedal gaits involve the coordinated movement of multiple joints, including the ankle, knee, and hip, as well as the interaction of the musculoskeletal system and the central nervous system. The foot must make contact with the ground in a manner that provides stability and propulsive forces, while also allowing for the transfer of energy from one limb to the other. These gaits can be found today mainly in birds and in earlier times in theropod dinosaurs, which also represent the greatest diversity of bipedal runners. Humans and most birds² walk at slow speeds and run at fast speeds. [24] Some great apes and monkeys are volitional bipeds, but usually only for rather short distances. At top speed, some lizards [17] and cockroaches [8] can bring their bodies into an almost upright posture and thus achieve bipedal running movements, increasing speed by expanding stride length. In general, bipeds achieve greater absolute stride lengths than quadrupeds of the same body mass [32]. This has been argued to be an advantage for endurance runners as our own species, for example while engaging in persistence hunting quadrupeds or aggressive scavenging in competition with them [4].

2.2 Gait Analysis

Gait analysis is the systematic study of walking patterns and movements, with the goal of understanding the mechanics of walking and, in the field of robotics, developing control algorithms to improve the robot's stability and balance. From a motor control perspective, bipedal gaits are thought to be controlled by a combination of reflexive and voluntary mechanisms, with the former providing stability and the latter allowing for intentional changes in gait patterns. A wide variety of models has been developed to analyze terrestrial locomotion, which can be classified based on the phase relationship of the kinetic and potential energy oscillations. The two most influential models for gait analysis for bipedal, quadrupedal, and multi-legged locomotion are the spring-loaded inverted pendulum (SLIP) model for running, where the energy oscillations are in phase, i.e. the kinetic and potential energy both reach a minimum at mid-stance, and the rigid inverted pendulum (RIP) model for walking, where the energy oscillations are out of phase. [24] Both methods model the subject as a point mass with oscillating legs, which allows the neglect of rotations around the CoM [18]. In bipedal gaits, ~~like that of humans~~, the leading foot represents the braking force and serves as an anchor point for the body's next movement. In contrast, the trailing foot represents the propulsive force that adds energy to the system to vault over this same anchor point. The CoM reaches its lowest point in mid-stance when running, i.e. the minimum potential energy, and the provisional highest point when walking, i.e. the maximum potential energy. Since braking occurs in the first half of a leg's stance phase and propulsion in the second half, the CoM velocity, i.e. the kinetic energy, reaches its minimum at mid-stance for both walking and running. [24] Figure 2.2 shows a schematic representation of the characteristic m-shape of the vertical GRF of a steady-state stance-phase pattern of a bipedal spring-mass model.

2.2.1 Spring-Loaded Inverted Pendulum

The SLIP model represents the body of a walker as a pendulum that is mounted on a spring and inverted, where the body acts as a mass-spring system and is supported by the ground

²Except small songbirds, which typically have more of a hopping than walking gait [24].

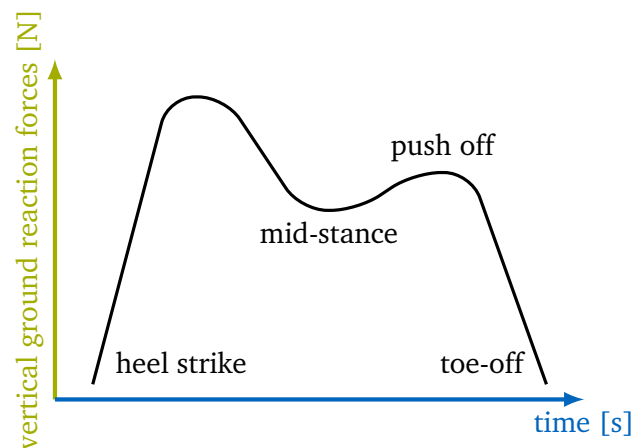


Figure 2.2: Schematic representation of the stance-phase pattern with its characteristic m-shape of the vertical GRF of a bipedal spring-mass model. The steady-state solution starts at heel strike, has a local minimum at mid-stance and ends at toe-off.

reaction force. The pendulum represents the CoM of the body, assumed as a point mass, and the massless spring serves as the ankle joint and its associated muscles and tendons in the legs, i.e. the model treats the phase of the stride in which the CoM is vaulting over the stance foot as an inverted pendulum with springs added inline to the legs. Since the springs are able to store energy during collision with the ground (i.e. during heel strike) and return it to the CoM during toe off, this model is typically found in running gaits. [3] SLIP-like gaits include bipedal running and hopping, as well as quadrupedal and multi-legged trotting, often described as "bouncing" gaits as the greatest leg compression occurs at about the same time as the greatest vertical force [27]. This spring-based gait can also be seen in animals that frequently hop, such as kangaroos. When physical springs are present, energy savings can be achieved via elastic storage and proportional return of absorbing and generative work performed by muscles or actuators. Overall, the SLIP model is a simple, yet quantitative way to represent the dynamics involved in walking and running and to analyze the energy economy describing the mechanical work done by the muscles and tendons. [3]

2.2.2 Rigid Inverted Pendulum

In the RIP model, the body of the walker is represented as a rigid rod that is inverted and balanced on a pivot point. The rod represents the body's CoM, and the pivot point represents the ankle joint. The body is subjected to gravitational forces that cause it to oscillate back and forth as it moves forward. According to the conventional interpretation of "two basic mechanisms", which states that the potential energy tends to reach a maximum near mid-stance during walking, it is sufficient to describe walking dynamics with a RIP-model derived using Lagrangian mechanics and non-linear equations of motion. The system is considered to be under-actuated because the control inputs are limited to the forces and torques at the ankle and knee joints. [24] Nonetheless, experimental studies show that bipedal and quadrupedal walking dynamics (e.g. [21], [13], [11]) do not reflect RIP-like behavior well. This is unsurprising given that an actual rigid inverted pendulum (i.e., a mass on a massless rod of fixed length) would show a peak vertical force instead of a minimum vertical force in the mid-stance position, as described by Geyer, Seyfarth, and Blickhan [12]. The authors presented an alternative walking model for compliant legs, called the bipedal spring-loaded inverted pendulum (BSLIP) model, which is described in more detail in the following section.

2.2.3 Bipedal Spring-Loaded Inverted Pendulum

The bipedal spring-loaded inverted pendulum (BSLIP) model, proposed by Geyer, Seyfarth, and Blickhan, is a variation of the SLIP model specifically designed to study bipedal walking gaits. The model is able to reproduce a similar m-shape of the vertical GRF as shown in figure 2.2 by providing a spring-loaded leg that introduces compliance. In addition, the model aggregates the leading and trailing leg forces during double support of the step-to-step transition. Although the BSLIP-model is widely used and frequently cited, it has not yet challenged the RIP-model in most textbooks. This may be in part because the BSLIP is more difficult to simulate and perhaps also because its conservative leg springs limit its ability to achieve the full range of human walking speeds. [25] Nevertheless, SLIP-like running and BSLIP-like walking were successfully demonstrated on a bipedal robot using the same spring-loaded legs for both gaits [16]. Theoretically, the BSLIP represents a more lifelike model because, unlike the rather unrealistic impulsive stride-to-stride transition of the RIP model, it is able to capture the characteristic m-shape of the GRF profile and, moreover, allows for double support [24].

2.2.4 Mechanical Cost Analysis

The mechanical cost analysis (MCA) is a method used to quantify the energy consumption and efficiency of movement patterns in biological and artificial systems. The goal of this analysis is to quantify the amount of energy required to perform a given task, such as walking or running, and to understand how different factors, such as speed, terrain, and body size, influence the energy cost. It involves calculating and comparing the mechanical work done by the system, i.e. the force applied to and the displacement of the system, as well as the metabolic energy consumption, to quantify the overall efficiency of the movement. MCA is widely used in fields such as biomechanics, sports science and robotics where it is important to understand the energy consumption and efficiency of movement patterns. In biomechanics, ~~for example~~, mechanical cost analysis can be used to study the energy consumption of different walking styles, while in robotics it can be used to optimize the energy efficiency of bipedal robots. The mechanical cost of transport (CoT_{mech}) can be decomposed into several components, including the work done against gravitational forces, work done against inertial forces, work done against frictional forces, and work done to change the velocity of the body segments. These components can be calculated using principles from mechanics, such as work-energy, impulse-momentum, and conservation of energy. The CoT_{mech} can also be influenced by various factors, such as body size and shape, limb coordination, and actuator activation patterns. For example, taller agents generally have a higher CoT_{mech} than shorter individuals just because they have to overcome larger gravitational forces. [2]

Based on this Lee et al. developed a collision-based approach, which uses the same point mass model as SLIP-based methods, but describes the locomotion directly by analyzing the force and velocity vectors. Unlike SLIP-based approaches, which are only approximations of a gait, the collision-based approach has the advantage that no *a priori* model needs to be known, which holds the potential to distinguish different gaits as well as to discern their defined characteristics [22].

Fundamental Determinants of Center of Mass Dynamics

The central concept of MCA is D'Alembert's [6] 'principle of orthogonal constraint', which shows that a mass can be redirected without mechanical work, as long as the constraint

(i.e. the force vector) is perpendicular to the path (i.e. the velocity vector), such that their dot-product (i.e. the mechanical power) is zero. However, this theoretical redirection with zero work cannot be implemented in real legged systems as terrestrial locomotion requires intermittent, discrete footfalls, which, among other things, constrains their ability to exert orthogonal forces by a leg's position with respect to the CoM, their kinematic range of motion and their force-torque capacity [24]. These "inelastic" collisions [20] by the limb with the ground preclude a consistent orthogonal relationship between the force and velocity vector, as their corresponding instantaneous angles θ (relative to vertical) and λ (relative to horizontal) [23] are of the same sign³, as shown in Figure 2.3a. This results in a non-zero collision angle ϕ and abrupt, collision-like changes in the CoM direction, which require mechanical work [22]. However, in the theoretical case, if the two vectors are perpendicular to each other, $\phi = 0$, meaning the angles θ and λ are equal and of opposite sign, which in turn means that no collision occurs, thus no work is done at the CoM, as for a wheel without rim but infinite spokes [2], as shown in 2.3b.

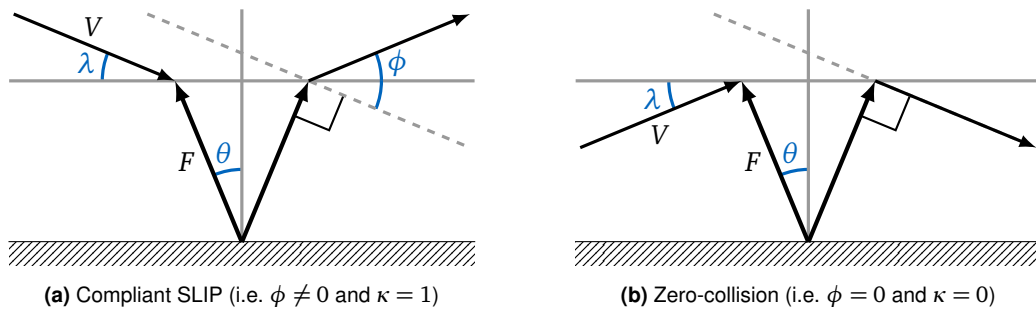


Figure 2.3: Schematic representation of the mechanical cost analysis (MCA) for a compliant SLIP (a) as well as the idealized zero-collision case (b). Shown are the force vector F and velocity vector V with their corresponding angles, θ and λ of two isolated, hypothetical strides. The collision angle ϕ is the deviation of the orthogonal relation between F and V . The collision reduction is quantified by the collision fraction κ . (Adapted from [22], p. 4)

To enforce the principle of orthogonal constraint, that is, to keep the force and velocity vectors of the CoM as orthogonal as possible, both metrics must be measured at each instant of the stride. If this orthogonal relationship is violated, either generative or absorptive costs are incurred, depending on the sign of the collision angle ϕ , which is the summation of the force and velocity angles θ and λ . If ϕ is less than 90 degrees, the cost is generative, i.e., the two vectors point somewhat in the same direction and energy can be applied to move forward. Conversely, if the angle is greater than 90 degrees, the cost and energy are absorptive, as is the case with deceleration. Theoretically, provided both vectors are always exactly 90 degrees out of phase, it would hereby be possible to redirect the CoM with zero work. [24] The power of the limb acting on the CoM of the body, i.e. the external mechanical power, can thus be quantified as

$$P_{mech} = F \cdot V \sin(\phi) \quad (2.1)$$

where F denotes the respective ground reaction force (GRF) vector, i.e. the external force acting on the limb, and V the velocity vector of the CoM. The mechanical work performed corresponds to the cumulative time integral over the duration of the impulse of the external mechanical power [7] [22]:

³This is consistent with compliant SLIP mechanics

$$W_{mech} = \int P_{mech} dt. \quad (2.2)$$

Center of Mass Velocities

Another common dimensionless unit for comparing moving objects is the Froude number (Fr). It can be used to classify walking gaits into different categories based on the relative importance of inertial and gravitational forces in the motion of the body. For example, when $Fr < 1$, the walking gait is characterized by stability-seeking behavior, while when $Fr > 1$, the walking gait is characterized by energy-saving behavior. The dimensionless velocity is the square-root of the Froude number. [1] [22]

$$\sqrt{Fr} = \sqrt{\frac{\bar{V}_y^2}{gh}} = \frac{\bar{V}_y}{\sqrt{gh}} \quad (2.3)$$

where \bar{V}_y depicts the average forward velocity, g the acceleration due to gravity and h the height of the CoM of the body.

Collision-Based Angles

The instantaneous collision angle ϕ is the deviation of perpendicularity of force and velocity vectors of the CoM [22], which is measured at each instance of the step and given by

$$\phi = \arcsin\left(\frac{\sum |F \cdot V|}{\sum |F||V|}\right). \quad (2.4)$$

The collision angle over the contact periods of the entire stride Φ is given by the weighted average of ϕ , where the weights represent the magnitude of the force and velocity vectors at each instant:

$$\Phi = \frac{\sum |F||V|\phi}{\sum |F||V|}. \quad (2.5)$$

Substituting using the small angle approximation of equation 2.4 into equation 2.5, that is, when only small vertical undulations and fore-aft forces appear, shows that the collision angle Φ is a close approximation to the mechanical cost of transport (CoT_{mech}) [22] as can be seen in

$$CoT_{mech} = \frac{\sum |F \cdot V|}{n\bar{V}_y mg} = \frac{\sum |F \cdot V|}{\sum |F||V|} \quad (2.6)$$

where the CoT_{mech} is a dimensionless metric of the normalized mechanical power during the contact period of the gait when the limb redirects the CoM [23], i.e. the mechanical work at the center of mass (CoM) required to move a unit body weight a unit distance in the direction of travel [22] [5] and n is the number of samples in the stride period.

Collision Fraction

The collision reduction is directly correlated to the collision angle Φ and quantified by the collision fraction κ , which gets small if either the velocity angle Λ^4 or the force angle Θ is small, if there is a near perpendicularity of the velocity vector V and the force vector F throughout the stride or any combination thereof. The collision fraction is the actual collision relative to potential collision:

$$\kappa = \frac{\Phi}{\Lambda + \Theta}. \quad (2.7)$$

For compliant SLIP, $\phi = \lambda + \theta$, since the braking force yields a non-perpendicular angle with downward velocity whereas the propulsive force yields one with upward velocity, resulting in an instantaneous $\kappa = 1$, shown in figure 2.3a. Whenever F and V are oriented in the same direction, collisions are reduced and $\kappa < 1$ up to the idealized case in which F and V remain orthogonal throughout the entire stride and thus $\phi = |\lambda - \theta|$, leading to $\kappa = 0$, shown in 2.3b. [22]

2.3 Summary

Locomotion is equally fundamental to all living things. Nature provides a myriad of ~~inspi-~~
~~rations as~~ various biological forms and functions to maneuver energy efficiently, agilely and safely through even the most hazardous environments evolved over the course of millions of years of evolution. [24] The analysis of terrestrial locomotion in the last half century has focused mainly on strategies for mechanical energy recovery during walking and running [22]. Legged locomotion can be classified in symmetrical and asymmetrical gaits, according to the phase relationship of the left-right pairs of legs, regardless of the number of pairs. A common definition depicts that symmetrical gaits involve both legs on the same side moving together whereas asymmetrical gaits involve diagonal pairs of legs moving together. ~~A wide variety of models has been developed to analyze terrestrial locomotion,~~ which can be classified based on the phase relationship of the kinetic and potential energy oscillations. The two most influential models for gait analysis for bipedal, quadrupedal, and multi-legged locomotion are the spring-loaded inverted pendulum (SLIP) model for running, where the energy oscillations are in phase, i.e. the kinetic and potential energy both reach a minimum at mid-stance, and the rigid inverted pendulum (RIP) model for walking, where the energy oscillations are out of phase. [24] Energy consumption and efficiency of movement patterns in biological and artificial systems can be quantified with the mechanical cost analysis (MCA). This method involves calculating and comparing the mechanical work done by the system, i.e. the force applied to and the displacement of the system, as well as the metabolic energy consumption, to quantify the overall efficiency of the movement. [2]

⁴Which tends to be greater in SLIP-like gaits such as running, hopping or trotting due to increased vertical oscillations of the CoM during these "bouncing gaits" [23].

Chapter 3

Solution approach

A MATLAB® Simulink [26] implementation of the JenaFox model, reflecting the test environment described in the upcoming section 3.1, was provided. A modified neural network controller based on the work of Geng, Porr, and Wörgötter [10] was used as controller, which is discussed in more detail in section 3.2. The concept of vertical leg orientation (VLO), proposed by Rummel et al. [33] and described in section 3.3, was taken as initial and final condition, i.e. one iteration of the simulation consists of one full step or one half of a stride, respectively. The iterations were finally analyzed using a trajectory optimization, described in section 3.4, in order to ~~end-up-with~~ a solution that is as periodic as possible, in other words, with as little difference as possible between the final and initial conditions of the robot.

3.1 The JenaFox Bipedal Walking Robot

JenaFox refers to a bipedal robot developed at the Jena University of Applied Sciences in Germany, designed for research in robotics and control engineering with a focus on bipedal locomotion. The robot resembles two human-like legs, connected by a torso, that are capable of walking and navigating different terrains. The system is equipped with a variety of sensors, such as accelerometers and gyroscopes, which provide data on its motion and orientation. This data can then be used to control the robot's actuators and thus its movements, allowing it to balance, walk, and respond to its environment in real-time. The robot is also designed to be highly scalable and modular, with a wide range of interchangeable components that can be customized to meet specific research needs. This includes the ability to easily swap out different sensors, actuators, and control boards, allowing researchers to easily experiment with different configurations and components. [28]

The robotic test environment is unique in that it is designed as an open-source platform, making it accessible to researchers and students who want to study and experiment with bipedal robotics. Overall, JenaFox is a valuable tool for researchers and students in the field of robotics and control engineering, as it provides a platform for exploring the challenges and opportunities associated with bipedal locomotion, and for developing new technologies and control strategies for robots. [28]

A schematic representation of the JenaFox robot is shown in figure 3.1a. The bipedal robot consists of a torso connected to two segmented legs, each of which has an upper and a lower link. When taking a step, the stance leg supports the weight of the robot, while the swing leg is free to move above the ground. All limbs are connected via actuators, with sensors in each joint measuring angular position and velocity, except for the ankle joint,

which is the only passive joint of the system. The trunk of the robot is attached to a boom via a freely rotating joint. The tether mechanism constrains the motion of the robot on a sphere, without excessively affecting its dynamics in the sagittal plane. The mechanism consists of an aluminum tube, a spherical pivot fixed to the floor and a tension cable. The tether is instrumented to provide measurements of the machine's three motions: vertical translation, forward translation, and rotation about the axis of the boom. [28] [29]

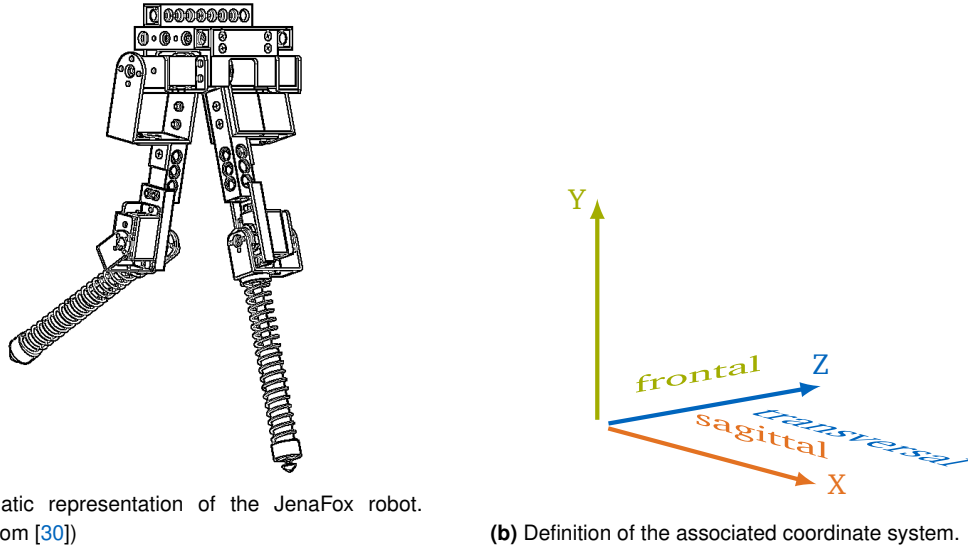


Figure 3.1: Schematic representation of the JenaFox bipedal walking robot (a) with associated planes of motion (b). The bipedal robot consists of a torso connected to two segmented legs, each of which has an upper and a lower link. The X-axis (orange) points in the direction of motion, the Y-axis (green) points upward. The trunk of the robot is attached to a boom via a freely rotating joint which constrains the motion of the robot on a sphere. The planar motion is thus restricted to the sagittal plane (orange).

The simulation of the JenaFox robot is created in MATLAB[®] Simulink R2022a as a Simscape multi-body model. The solver settings used for the simulation are listed in table 3.1.

Table 3.1: Solver settings for the JenaFox robot MATLAB Simulink simulation.

Solver setting	Value
Solver type	variable-step
Solver	ode23s (Min./ Rosenbrock)
Max step size	0.1
Min step size	auto
Relative tolerance	0.01
Absolute tolerance	0.001

3.2 Neural Network Controller





In the simulation, a neural network controller based on the work of Geng, Porr, and Wörgötter [10] was used. The authors propose that a bio-inspired neural network controller may perform better in biped control than other comparable solution methods, such as zero moment point or inverted pendulum control, as it guarantees a stable gait even at high speeds.

A Neural Network Controller is a type of artificial intelligence algorithm that uses the principles of artificial neural networks to control the behavior of a system. Neural networks are modeled after the structure and function of the human brain, and they are trained using large amounts of data to learn how to perform a particular task. In the context of a neural network controller, the network is trained to produce control signals for a system based on inputs that represent the state of the system. These inputs could include sensor readings, past control signals, or other relevant information about the system. The neural network then outputs control signals that are used to regulate the behavior of the system. One of the key benefits of using a neural network controller is that, despite being highly scalable and flexible, it can learn to perform complex tasks that are difficult to describe mathematically. For example, a neural network controller could be trained to control a robot to walk, swim, or fly in a way that is similar to how animals perform these tasks. The network can learn from examples and adapt to new situations, making it well-suited for tasks that are subject to unpredictable variations or changing conditions. [10]

Despite its many benefits, there are also some challenges associated with using a neural network controller. One of these challenges is that it can be difficult to interpret how the network is making decisions, since the internal workings of the network are often highly complex and non-linear. ~~This can make it difficult to understand why the network is behaving in a certain way, or to identify and correct errors in the network's behavior.~~ Another challenge is that neural networks are often trained using large amounts of data, ~~and this can be computationally intensive and time consuming.~~ This can make it difficult to use neural network controllers in real-time applications, where the control signals need to be generated quickly and with a high level of accuracy. [10]

Figure 3.2 shows the control parameters used for the joint angles according to the International Society of Biomechanics (ISB)¹ convention. The parameter set consists of eight angles and five voltage values, i.e. for both the left and right leg two extreme angles each for hip and knee with respective voltage values for extension and flexion of each joint. The fifth voltage value represents the hold voltage of the knee in stance to keep the leg straight. An overview of the used control scheme is given in table 3.2.

Table 3.2: Overview of the control scheme used for the JenaFox robot. Touchdown and reaching the anterior extreme angle (AEA) of either hip angle triggers the corresponding action. When the target is reached the power of the moving motors is switched off. In the images, the events are shown as dark stick figures and the corresponding actions as light stick figures. (Adapted from [29], p.36)

Event	1. TD _r		2. HL@AEA		3. TD _l		4. HR@AEA	
	action	goal	action	goal	action	goal	action	goal
left hip (HL)	flex	AEA			extend	PEA		
left knee (KL)	flex	PEA	extend	AEA	hold	AEA		
right hip (HR)	extend	PEA				flex	AEA	
right knee (KR)	hold	AEA			flex	PEA	extend	AEA
								
	L R		R L		R L		L R	

¹The International Society of Biomechanics (ISB) is a non-profit organization founded in 1973 dedicated to promoting the study and application of biomechanics around the world.

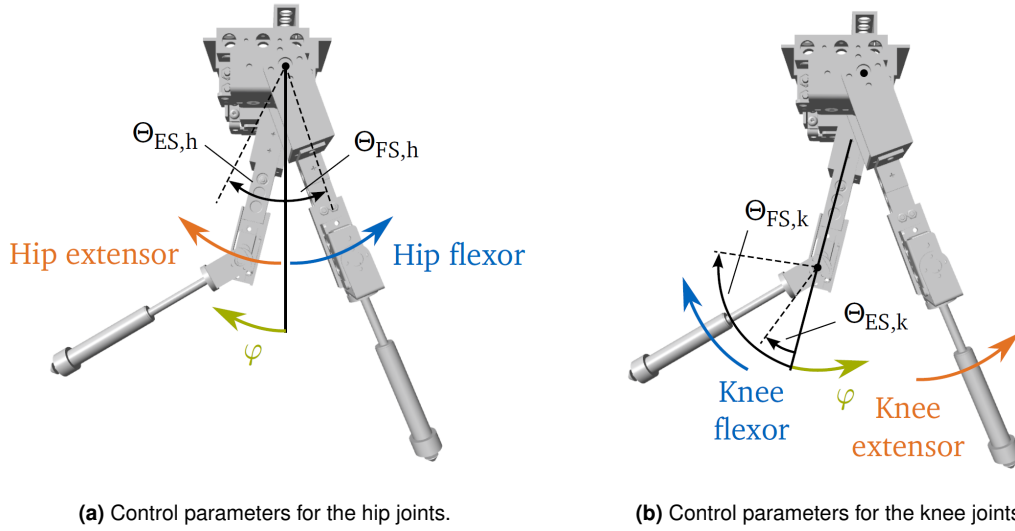


Figure 3.2: The control parameters for the hip (a) extensor $\theta_{ES,h}$ (orange) and flexor $\theta_{FS,h}$ (blue) as well as the knee (b) extensor $\theta_{ES,k}$ (orange) and flexor $\theta_{FS,k}$ (blue) joint angles according to the International Society of Biomechanics (ISB) convention. (Adapted from [31])

A summary of the control parameters is given in table 3.3 and table 3.4, where the AEA is obtained with a sigmoid function², known for its characteristic "S"-shaped sigmoid curve, as

$$AEA = \frac{-15}{1 + e^{k \cdot \lambda_{proj} + d}} - 10 \quad (3.1)$$

where k depicts a proportionality constant, λ_{proj} the projected velocity vector, i.e. the velocity vector of the CoM λ_{com} projected down to the hip and d is an offset, i.e. a shift of the function along the x-axis. Values of $k = -0.3$ and $d = 7$ were chosen to map the values of λ_{proj} to obtain values of the anterior extreme angle (AEA) between -10° and -25° , as shown in the following figure 3.3

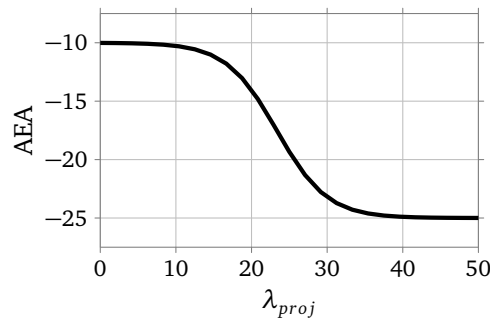


Figure 3.3: Graphical representation of equation 3.1. The sigmoid function maps the projected velocity vector λ_{proj} to obtain the anterior extreme angle (AEA).

The anterior extreme angle (AEA) by definition corresponds to the angle of attack α_{TD} , i.e.

$$\alpha_{TD} = AEA \quad (3.2)$$

²The sigmoid function is a mathematical function commonly used in machine learning and neural networks, where it can be used as a type of activation function that maps any real-valued number to a value between 0 and 1, which makes it useful for modeling probabilities and binary classification problems.

Table 3.3: Overview of the used control parameters for the sensory neurons, i.e. the joint angles of the hip extensor $\theta_{ES, h}$ and flexor $\theta_{FS, h}$ as well as the knee extensor $\theta_{ES, k}$ and flexor $\theta_{FS, k}$.

Control parameters for sensory neurons	Description	Value	Unit
$\theta_{ES, h}$	Threshold for hip extensor	5	[°]
$\theta_{FS, h}$	Threshold for hip flexor	AEA	[°]
$\theta_{ES, k}$	Threshold for knee extensor	-3	[°]
$\theta_{FS, k}$	Threshold for knee flexor	-80	[°]

Table 3.4: Overview of the used control parameters for the motor neurons. τ is a time constant associated with the passive properties of the cell membrane, M_{AMP} represents the magnitude of the servo amplifier. GM_h and GM_k depict the gain of the hip and knee motor, respectively.

Control parameters for motor neurons	Description	Value	Unit
τ	Time constant	0.01	[s]
M_{AMP}	Magnitude of the servo amplifier	3	—
GM_h	Gain of the hip motor	1.0 - 1.8	—
GM_k	Gain of the knee motor	$0.9 \cdot GM_h$	—

τ is a time constant associated with the passive properties of the cell membrane [9] and M_{AMP} represents the magnitude of the servo amplifier [10]. In the course of this work, the gain of the hip motor GM_h was modulated in the range between 1.0 and 1.8 in steps of 0.2. The initial velocities of the CoM were set via the following equation 3.3, which are graphically shown in figure 3.4:

$$\begin{aligned} dx_{CoM} &= 0.45 \cdot GM_h + 0.02 \\ dy_{CoM} &= -0.23 \end{aligned} \quad (3.3)$$

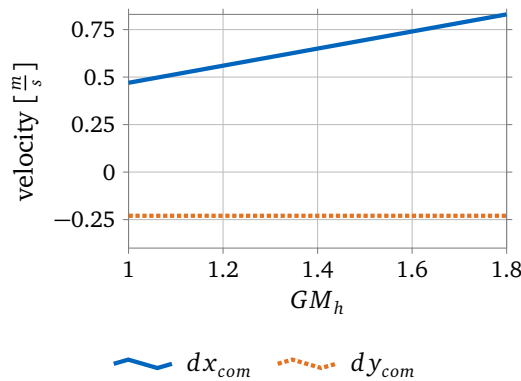


Figure 3.4: Graphical representation of equation 3.1. The sigmoid function maps the projected velocity vector λ_{proj} to obtain the anterior extreme angle (AEA).

3.3 Vertical Leg Orientation

The vertical leg orientation (VLO) refers to the orientation of the leg of a bipedal robot relative to the ground and is defined as the angle between the vertical axis (perpendicular to the ground) and the line connecting the foot and hip joint of the robot. In a normal walking gait, the VLO changes throughout the stride cycle as the robot moves from one foot to the other. During the stance phase, the VLO starts at a relatively small angle, increases as the robot transfers weight over the stance leg, and reaches its maximum value just before the swing phase. During the swing phase, the VLO decreases as the swing leg moves forward, reaches its minimum value just before the footstrike, and then increases again as the swing leg moves into the stance phase. [33]

The JenaFox robot is capable of periodic gait patterns such as walking and running, where a gait pattern is fully described by the system parameters and initial conditions. In the course of this work, the initial conditions are chosen so that the stance leg is in contact with the ground and vertically oriented, i.e. the CoM is exactly above the foot point ($x = x_{FP_1}$), meaning that the horizontal position is zero with respect to the actual foot point. A single step is completed when the swing leg attains ground contact and the CoM is orthogonally above the second foot point ($x = x_{FP_2}$), as shown in figure 3.5. The simulation starts at the moment of vertical leg orientation (VLO) during single support phase (VLO_0) and ends after one step is completed at VLO of the opposite leg (VLO_1). These initial conditions can be used to reduce the number of independent initial conditions. [33]

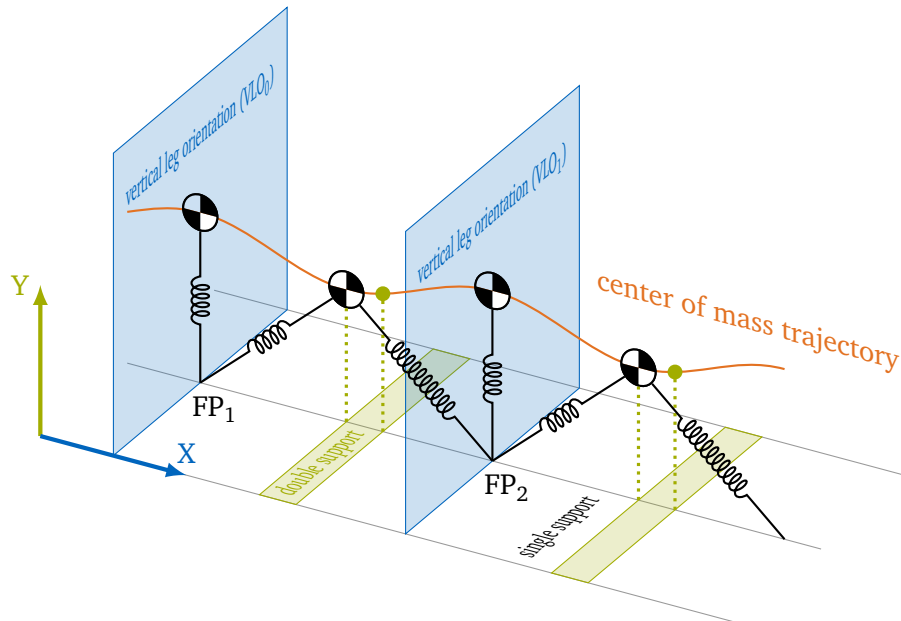


Figure 3.5: The bipedal spring mass model for walking. The simulation starts at the moment of vertical leg orientation (VLO) during single support phase (VLO_0) and ends after one step is completed at VLO of the opposite leg (VLO_1). (Adapted from [33], p. 1)

3.4 Trajectory Optimization

Trajectory optimization is a method for designing the motion of a system to achieve a desired goal. It involves the calculation of an optimal path taking various constraints and objectives

into account. The term trajectory refers to the path an agent travels as a function of time. The term trajectory optimization is therefore the set of methods used to obtain the best trajectory, usually by selecting appropriate inputs to the system, i.e. controls, as functions of time. The comprehensive policy of optimization is to minimize the objective function subject to a number of constraints and restrictions. [19] In the course of this work a trajectory optimization was performed via finding a minimum of constrained nonlinear multivariable functions.

The process typically involves the following steps [19]:

1. Modeling the robot's dynamics: A mathematical model of the robot's movement is created, which takes into account the robot's kinematics, dynamics, and control inputs.
2. Specifying the constraints: The constraints that must be satisfied by the robot's motion are defined, such as bounds on the joint angles and torques, as well as collision avoidance constraints.
3. Defining the objective: The objective function to be optimized is defined, which might include a trade-off between energy efficiency, speed, and smoothness of motion.
4. Solving the optimization problem: An optimization algorithm is applied to find the path that minimizes the objective function while satisfying the constraints.
5. Generating the motion trajectory: The optimal path is transformed into a set of points that define the motion trajectory for the robot.

The following sections describe the individual steps that were carried out in more detail.

Assumptions

Within this work it is assumed that the trajectory is single-phase and of continuous time, meaning the system dynamics are continuous throughout the entire trajectory. The dynamics, objective and constraints are smooth, consistent and potentially non-linear. Furthermore, the robot is considered to be left-right symmetric, allowing to search for a periodic walking gait with a single step instead of a stride. A periodic gait requires that the joint trajectories, consisting of the joint angles, their rates and the associated torques, are the same for each successive step. [19]

Constraints

The first and possibly most important constraint is the system dynamics. In addition, limits are defined for the boundary condition, restricting the initial and final states of the system, including upper and lower limits for the joint angles and joint velocities. In addition, the initial state was limited to the VLO, i.e. the stance leg always starts vertically oriented.

Nonlinear Programming

Most direct collocation methods transcribe a continuous-time trajectory optimization problem into a nonlinear program (NLP), i.e. a constrained parameter optimization problem that has nonlinear terms in either its objective or its constraint function. This nonlinearity makes NLP

problems more difficult to solve, as the objective function and/or constraints can have multiple local minima (or maxima) and the global minimum (or maximum) may not be easily accessible. [19] A common formulation for a nonlinear program is as follows:

$$\begin{aligned} \min_x \quad & f(x) \\ \text{subject to} \quad & h(x) = 0 \\ & g(x) \leq 0, \\ & x_l \leq x \leq x_u \end{aligned} \tag{3.4}$$

where x denotes the vector of design variables, $f(x)$ the objective function, $h(x)$ the equality constraint functions, $g(x)$ the inequality constraint functions and x_l, x_u the lower and upper bounds, respectively.

System Dynamics

During single support (see figure 3.5), the system has five degrees of freedom (DoF): the absolute angles of both lower legs, i.e. of the knee joints (q_5 and q_7), both upper legs, i.e. of the hip joints (q_4 and q_6) as well as the torso (q_3), as can be seen in figure 3.6.

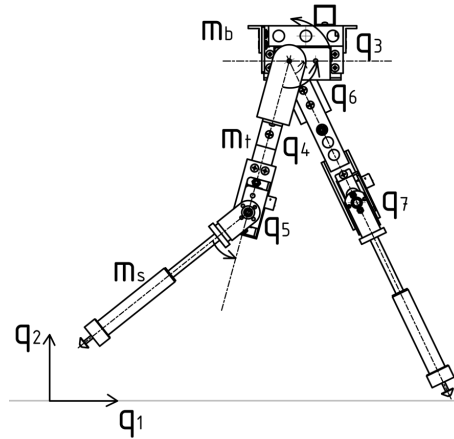


Figure 3.6: Degrees of freedom of the basic mechanical setup. The trunk (mass m_b) has three degrees of freedom (q_1, q_2, q_3), hip and knee of the right leg connect the thigh (m_t) to the body and shank (m_s) to the thigh respectively by one degree of freedom each (q_4, q_5), the same counts for the left side (q_6, q_7). (Adapted from [29], p.37)

Hereafter, the DoF of the system are cumulated into the single vector q . Since it is a second order dynamical system, the derivative of the configuration, \dot{q} must also be included. Thus, the state and dynamics can be described as:

$$x = \begin{bmatrix} q \\ \dot{q} \end{bmatrix}, \quad \dot{x} = f(x, u) = \begin{bmatrix} \dot{q} \\ \ddot{q} \end{bmatrix} \tag{3.5}$$

where q are the angles, \dot{q} the angular rates and \ddot{q} the accelerations, respectively. Since the initial and final state of the optimization problem are defined using the VLO, the stance leg is always ~~vertically~~ oriented. Thus, the respective hip and knee angles as well as the corresponding angular velocities can be neglected. This results in six parameters which have to be considered: The hip and knee angle of the swing leg, the angle of the upper body

and their angular velocities. Table 3.5 shows the initial condition used in the multi-body simulation.

Table 3.5: Initial condition used in the multi-body simulation consisting of the hip and knee angles of the swing leg, $\phi_{IC, hr}$ and $\phi_{IC, kr}$, the angle of the torso $\phi_{IC, torso}$ as well as their corresponding velocities $\dot{\phi}_{IC, hr}$, $\dot{\phi}_{IC, kr}$ and $\dot{\phi}_{IC, torso}$.

Initial conditions	Description	Value	Unit
$\phi_{IC, kr}$	Angle of the right knee	-40	[°]
$\phi_{IC, hr}$	Angle of the right hip	15	[°]
$\phi_{IC, torso}$	Angle of the torso	0	[°]
$\dot{\phi}_{IC, kr}$	Angular velocity of the right knee	1.6 - 2.6	$[\frac{rad}{s}]$
$\dot{\phi}_{IC, hr}$	Angular velocity of the right hip	0.9 - 1.5	$[\frac{rad}{s}]$
$\dot{\phi}_{IC, torso}$	Angular velocity of the torso	0	$[\frac{rad}{s}]$

where $\dot{\phi}_{IC, kr}$ and $\dot{\phi}_{IC, hr}$ are calculated from the initial velocity of the CoM divided by the length of thigh and shank of the leg, respectively.

Objective Function

To ensure that the walking gait is periodic, the sum of absolute deviations between the initial and final state is used as the cost function. The states consist of q and \dot{q} , with the absolute value of the torso angle to allow the frequency of the torso to be potentially half the frequency of a full step.

$$f = \sum_{i=1}^5 |q(T)_i - q(0)_i|. \quad (3.6)$$

Further, the knee angle of the swing leg at touchdown is also included with an exponential penalty of the form

$$y = -50 \cdot (0.5^{|x|} - 1) \quad (3.7)$$

which converges to a penalty value of 50. This ensures the smallest possible knee angle and thus the most extended leg possible at touchdown. The same penalty was also applied to the final state of the hip and knee angle of the landing leg, to keep the angles as small as possible and thus to regain the upcoming VLO_1 to the greatest possible extent again. Choosing an appropriate cost function is desirable to obtain smooth, well-behaved solutions, ensuring good convergence of the nonlinear program. Among others, the CoT is widely used, which, however, is difficult to optimize over because the solutions tend to have discontinuities. [19]

Termination conditions

To increase the robustness of the model, possible error modes are identified in which the model shows unexpected or undesired behavior. The identified conditions are presented in table 3.6, such as the CoM or one of the knees falling below a threshold in height, the robot starting to walk backwards as well as reaching a time or distance limit. If any of these cases

occur, the simulation is aborted and the cost is penalized with a penalty function similar to the one used for the angles.

Table 3.6: Identified failure modes of the system which may occur. A total of 6 failure modes were identified, the CoM or one of the knees falling below a threshold in height, the robot starting to walk backwards as well as reaching a time or distance limit. If any of these cases occur, the simulation is aborted and the cost is penalized with a penalty function.

Failure Mode	Condition
Falling	$y_{com} \leq 0.15[m]$
Knee falling	$y_{knee_r}, y_{knee_l} \leq 0.028[m]$
Walking backwards	$\dot{x} \leq -10[\frac{m}{s}]$
Time limit	$time > 6.0[s]$
Distance limit	$distance > 0.5[m]$

3.5 Summary

In this chapter the individual steps, which are necessary to design a controller for the torso stabilization of a bipedal robot, are considered in detail. A Simulink implementation of the JenaFox model was provided. The used neural network controller is based on the work of Geng, Porr, and Wörgötter [10]. The initial and final condition is defined by the vertical leg orientation (VLO). In order to be able to evaluate the individual iterations, a trajectory optimization problem was formulated in which the best solution is also the most periodic one, i.e. the solution in which the difference between the initial state (VLO₀) and final state (VLO₁) is as small as possible.

Chapter 4

Evaluation

The overall goal is to obtain a control law via reverse engineering that answers the following question: How must the offset angle d be set to get a touchdown with the current state of the robot so that it becomes periodic again in the next step? The ideal case would be to find a constant offset which, independent of the velocity vector, always leads to a periodic solution. The first set of experiments was performed to the effect that d , i.e. the angle between the projected velocity vector λ_{proj} and the AEA, as shown in equation 3.1, was modulated. The desired effect here is to shift the AEA with the velocity vector λ_{proj} , i.e. the steeper λ_{proj} becomes, the steeper should also AEA become to consequently obtain a steeper angle of attack α_{TD} and thus exchange as much vertical for horizontal velocity as possible. The used motor gain GM_h was set to a fixed value of 1.5. Subsequently, the optimizer was left to find a solution as periodic as possible via the cost function from equation 3.6. However, it quickly became clear that it makes more sense to modulate the gain of the hip motor GM_h , since this straightly affects the output voltage of the motor, which is directly proportional to the velocity. Figure 4.1 shows the velocity vectors at touchdown. At the beginning of the velocity vectors the leg position is schematically shown, where the hip, knee and ankle joints are drawn as circles. From this it can be seen that the robot performs the touchdown with a fully extended knee. The colors refer to the different motor gains, with red representing the lowest with a GM_h of 1, and purple the highest with a GM_h of 1.8. The angle of the velocity vector λ_{proj} tends to get steeper the larger the motor gain GM_h , i.e. the faster the robot runs. A steeper velocity vector has more vertical than horizontal velocity and thus leads to a steeper angle of attack α_{TD} .

Figure 4.2 shows the velocity vectors at VLO. ~~At the beginning of the velocity vectors the leg position is schematically shown, where the hip, knee and ankle joints are drawn as circles.~~ A single step is completed when the swing leg attains ground contact and the CoM is orthogonally above the second foot point ($x = x_{FP_2}$). The colors refer to the different motor gains, with red representing the lowest with a GM_h of 1, and purple the highest with a GM_h of 1.8.

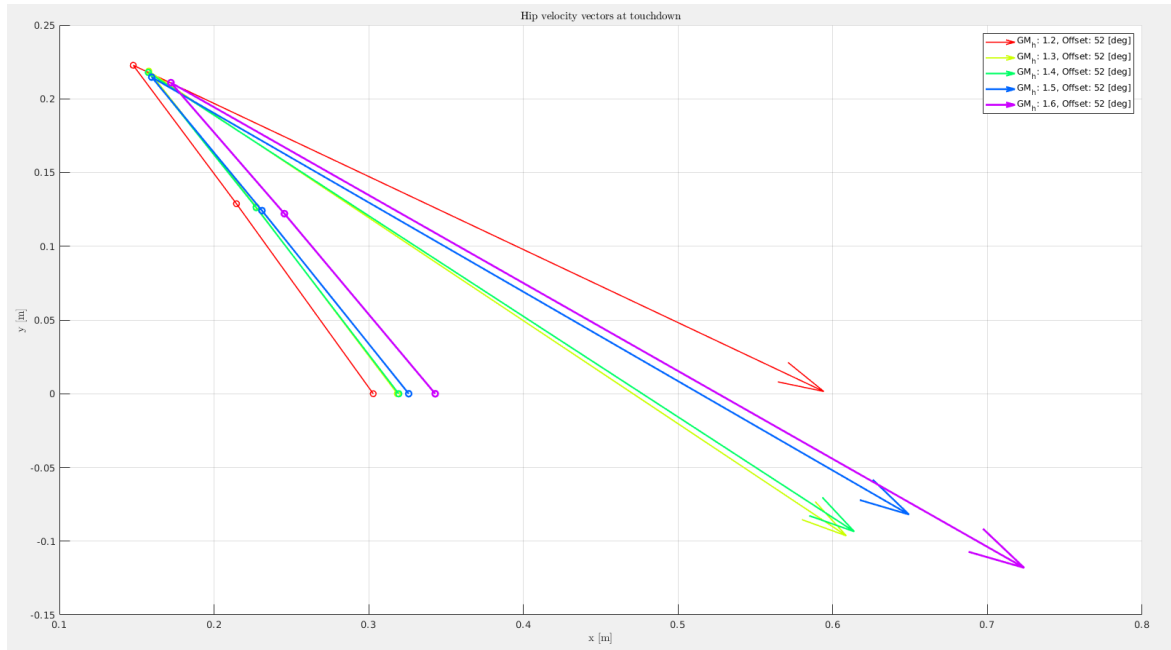


Figure 4.1: The velocity vectors at touchdown. At the beginning of the velocity vectors the leg position is schematically shown, where the hip, knee and ankle joints are drawn as circles. From this it can be seen that the robot performs the touchdown with a fully extended knee. The colors refer to the different motor gains, with red representing the lowest with a GM_h of 1, and purple the highest with a GM_h of 1.8.

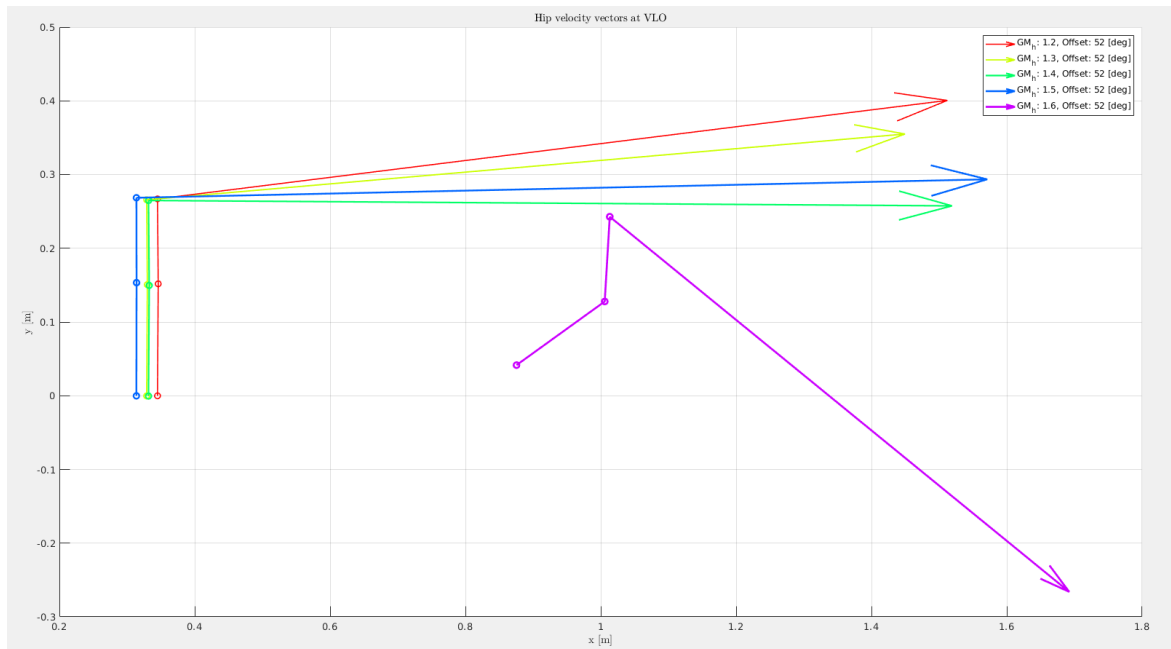


Figure 4.2: The velocity vectors at VLO. At the beginning of the velocity vectors the leg position is schematically shown, where the hip, knee and ankle joints are drawn as circles. A single step is completed when the swing leg attains ground contact and the CoM is orthogonally above the second foot point ($x = x_{FP_2}$). The colors refer to the different motor gains, with red representing the lowest with a GM_h of 1, and purple the highest with a GM_h of 1.8.

Chapter 5

Future work

Chapter 6

Conclusion

Appendix A

Appendix 1

Bibliography

- [1] Alexander, R. M. “The Gaits of Bipedal and Quadrupedal Animals”. In: *The International Journal of Robotics Research* 3.2 (June 1984), pp. 49–59. DOI: 10.1177/027836498400300205.
- [2] Andrew Biewener, S. P. *Animal Locomotion*. Oxford University Press, Mar. 23, 2018. 256 pp. ISBN: 0191060852. URL: https://www.ebook.de/de/product/34926791/andrew_biewener_sheila_patek_animal_locomotion.html.
- [3] Blickhan, R. “The spring-mass model for running and hopping”. In: *Journal of Biomechanics* 22.11-12 (Jan. 1989), pp. 1217–1227. DOI: 10.1016/0021-9290(89)90224-8.
- [4] Carrier, D. R., Kapoor, A. K., Kimura, T., Nickels, M. K., Scott, E. C., So, J. K., and Trinkaus, E. “The Energetic Paradox of Human Running and Hominid Evolution [and Comments and Reply]”. In: *Current Anthropology* 25.4 (Aug. 1984), pp. 483–495. DOI: 10.1086/203165.
- [5] Cavagna, G. A., Heglund, N. C., and Taylor, C. R. “Mechanical work in terrestrial locomotion: two basic mechanisms for minimizing energy expenditure”. In: *American Journal of Physiology-Regulatory, Integrative and Comparative Physiology* 233.5 (Nov. 1977), R243–R261. DOI: 10.1152/ajpregu.1977.233.5.r243.
- [6] D’Alembert, J. B. *Traité de Dynamique*. 1743.
- [7] Donelan, J. M., Kram, R., and Kuo, A. D. “Simultaneous Positive and Negative External Mechanical Work in Human Walking”. In: *Journal of Biomechanics* 35.1 (Jan. 2002), pp. 117–124. DOI: 10.1016/S0021-9290(01)00169-5.
- [8] Full, R. J. and Tu, M. S. “Mechanics of a rapid running insect: two-, four- and six-legged locomotion”. In: *Journal of Experimental Biology* 156.1 (Mar. 1991), pp. 215–231. DOI: 10.1242/jeb.156.1.215.
- [9] Gallagher, J. C., Beer, R. D., Espenschied, K. S., and Quinn, R. D. “Application of evolved locomotion controllers to a hexapod robot”. In: *Robotics and Autonomous Systems* 19.1 (Nov. 1996), pp. 95–103. DOI: 10.1016/S0921-8890(96)00036-x.
- [10] Geng, T., Porr, B., and Wörgötter, F. “Fast Biped Walking with a Sensor-driven Neuronal Controller and Real-time Online Learning”. In: *The International Journal of Robotics Research* 25.3 (Mar. 2006), pp. 243–259. DOI: 10.1177/0278364906063822.
- [11] Genin, J. J., Willems, P. A., Cavagna, G. A., Lair, R., and Heglund, N. C. “Biomechanics of locomotion in Asian elephants”. In: *Journal of Experimental Biology* 213.5 (Mar. 2010), pp. 694–706. DOI: 10.1242/jeb.035436.
- [12] Geyer, H., Seyfarth, A., and Blickhan, R. “Compliant leg behaviour explains basic dynamics of walking and running”. In: *Proceedings of the Royal Society B: Biological Sciences* 273.1603 (Aug. 2006), pp. 2861–2867. DOI: 10.1098/rspb.2006.3637.
- [13] Griffin, T. M., Main, R. P., and Farley, C. T. “Biomechanics of quadrupedal walking: how do four-legged animals achieve inverted pendulum-like movements?” In: *Journal of Experimental Biology* 207.20 (Sept. 2004), pp. 3545–3558. DOI: 10.1242/jeb.01177.

- [14] Hildebrand, M. "Symmetrical Gaits of Horses". In: *Science* 150.3697 (Nov. 1965), pp. 701–708. DOI: 10.1126/science.150.3697.701.
- [15] Hildebrand, M. "Symmetrical gaits of dogs in relation to body build". In: *Journal of Morphology* 124.3 (Mar. 1968), pp. 353–359. DOI: 10.1002/jmor.1051240308.
- [16] Hubicki, C., Abate, A., Clary, P., Rezazadeh, S., Jones, M., Peekema, A., Why, J. V., Domres, R., Wu, A., Martin, W., Geyer, H., and Hurst, J. "Walking and Running with Passive Compliance: Lessons from Engineering: A Live Demonstration of the ATRIAS Biped". In: *IEEE Robotics and Automation Magazine* 25.3 (Sept. 2018), pp. 23–39. DOI: 10.1109/mra.2017.2783922.
- [17] Irschick, D. and Jayne, B. "Comparative three-dimensional kinematics of the hindlimb for high-speed bipedal and quadrupedal locomotion of lizards". In: *Journal of Experimental Biology* 202.9 (May 1999), pp. 1047–1065. DOI: 10.1242/jeb.202.9.1047.
- [18] Kajita, S. and Tani, K. "Study of dynamic biped locomotion on rugged terrain-derivation and application of the linear inverted pendulum mode". In: *Proceedings. 1991 IEEE International Conference on Robotics and Automation*. IEEE Comput. Soc. Press. DOI: 10.1109/robot.1991.131811.
- [19] Kelly, M. "An Introduction to Trajectory Optimization: How to Do Your Own Direct Collocation". In: *SIAM Review* 59.4 (Jan. 2017), pp. 849–904. DOI: 10.1137/16m1062569.
- [20] Kuo, A. D., Donelan, J. M., and Ruina, A. "Energetic Consequences of Walking Like an Inverted Pendulum: Step-to-Step Transitions". In: *Exercise and Sport Sciences Reviews* 33.2 (Apr. 2005), pp. 88–97. DOI: 10.1097/00003677-200504000-00006.
- [21] Lee, C. R. and Farley, C. T. "Determinants of the center of mass trajectory in human walking and running." In: *Journal of Experimental Biology* 201.21 (Nov. 1998), pp. 2935–2944. DOI: 10.1242/jeb.201.21.2935.
- [22] Lee, D. V., Bertram, J. E. A., Anttonen, J. T., Ros, I. G., Harris, S. L., and Biewener, A. A. "A collisional perspective on quadrupedal gait dynamics". In: *Journal of The Royal Society Interface* 8.63 (Apr. 2011), pp. 1480–1486. DOI: 10.1098/rsif.2011.0019.
- [23] Lee, D. V., Comanescu, T. N., Butcher, M. T., and Bertram, J. E. A. "A comparative collision-based analysis of human gait". In: *Proceedings of the Royal Society B: Biological Sciences* 280.1771 (Nov. 2013), p. 20131779. DOI: 10.1098/rspb.2013.1779.
- [24] Lee, D. V. and Harris, S. L. "Linking Gait Dynamics to Mechanical Cost of Legged Locomotion". In: *Frontiers in Robotics and AI* 5 (Oct. 2018). DOI: 10.3389/frobt.2018.00111.
- [25] Lipfert, S. W., Günther, M., Renjewski, D., Grimmer, S., and Seyfarth, A. "A model-experiment comparison of system dynamics for human walking and running". In: *Journal of Theoretical Biology* 292 (Jan. 2012), pp. 11–17. DOI: 10.1016/j.jtbi.2011.09.021.
- [26] MATLAB. *version 9.12.0.2039608 (R2022a) Update 5*. Natick, Massachusetts: The MathWorks Inc., 2022.
- [27] McMahon, T. A. and Cheng, G. C. "The mechanics of running: How does stiffness couple with speed?" In: *Journal of Biomechanics* 23 (Jan. 1990), pp. 65–78. DOI: 10.1016/0021-9290(90)90042-2.
- [28] Renjewski, D. "Robotic Spring-Mass Walkers - Potential and Limitations". In: *Dynamic Walking*. 2012.
- [29] Renjewski, D. *An Engineering Contribution to Human Gait Biomechanics*. Verlag Dr. Kovac, 2013, p. 140. ISBN: 9783830068587.

- [30] Renjewski, D. [*Schematic representation of the JenaFox robot*]. [Applied Biorobotics (Module MW2388): Online; accessed January 22, 2023]. URL: <https://www.moodle.tum.de/course/view.php?id=75052>.
- [31] Renjewski, D. [*The extensor and flexor joint angles of the Jenafox robot*]. [Applied Biorobotics (Module MW2388): Online; accessed January 22, 2023]. URL: <https://www.moodle.tum.de/mod/page/view.php?id=2068770>.
- [32] Reynolds, T. R. “Stride length and its determinants in humans, early hominids, primates, and mammals”. In: *American Journal of Physical Anthropology* 72.1 (Jan. 1987), pp. 101–115. DOI: 10.1002/ajpa.1330720113.
- [33] Rummel, J., Blum, Y., Maus, H. M., Rode, C., and Seyfarth, A. “Stable and robust walking with compliant legs”. In: *2010 IEEE International Conference on Robotics and Automation*. IEEE, May 2010. DOI: 10.1109/robot.2010.5509500.
- [34] Siciliano, B. and Khatib, O., eds. *Springer Handbook of Robotics*. Springer International Publishing, 2016. DOI: 10.1007/978-3-319-32552-1.
- [35] Sitti, M., Menciassi, A., Ijspeert, A. J., Low, K. H., and Kim, S. “Survey and Introduction to the Focused Section on Bio-Inspired Mechatronics”. In: *IEEE/ASME Transactions on Mechatronics* 18.2 (Apr. 2013), pp. 409–418. DOI: 10.1109/tmech.2012.2233492.
- [36] Vernon, D. *Artificial Cognitive Systems. A Primer*. MIT Press, 2014, p. 288. ISBN: 9780262028387.